Insights into post-growth doping and proposals for CdTe:In photovoltaic devices

Journal of Physics: Energy

PAPER

Insights into post-growth doping and proposals for CdTe:In photovoltaic devices

Luke Thomas[1], Theo D C Hobson[1], Laurie J Phillips[1], Kieran J Cheetham[1,5], Neil Tarbuck[1], Leanne A H Jones[1], Matt J Smiles[1], Chris H Don[1], Pardeep K Thakur[2], Mark Isaacs[3], Huw Shiel[1,6], Stephen Campbell[4], Vincent Barrioz[4], Vin Dhanak[1], Tim Veal[1], Jonathan D Major[1] and Ken Durose[1,*]

[1] Department of Physics/Stephenson Institute for Renewable Energy, University of Liverpool, Liverpool, L69 7ZF, United Kingdom
[2] Diamond Light Source, Harwell Science & Innovation Campus, Didcot, Oxfordshire OX11 0DE, United Kingdom
[3] Harwell XPS, Research Complex at Harwell (RCaH), Didcot OX11 0FA, United Kingdom
[4] Department of Maths, Physics and Electrical Engineering, University of Northumbria, Newcastle-upon-Tyne NE1 8ST, United Kingdom
[5] Present Address: STFC, Daresbury Laboratory, Keckwick Lane, Daresbury, Cheshire WA4 4AD, United Kingdom.
[6] Present Address: Department of Materials, Imperial College London, Prince Consort Road, London SW7 2BP, United Kingdom.
[*] Author to whom any correspondence should be addressed.

E-mail: ken.durose@liverpool.ac.uk

Keywords: thin film solar cell, photovoltaics, cadmium telluride, n-type absorber, doping, indium

Supplementary material for this article is available online

OPEN ACCESS

RECEIVED
26 April 2022

REVISED
15 June 2022

ACCEPTED FOR PUBLICATION
21 June 2022

PUBLISHED
2 August 2022

Abstract

This paper is motivated by the potential advantages of higher doping and lower contact barriers in CdTe photovoltaic devices that may be realized by using n-type rather than the conventional p-type solar absorber layers. We present post-growth doping trials for indium in thin polycrystalline CdTe films using the diffusion of indium metal with indium chloride. Chemical concentrations of indium up to 10^{19} cm^{-3} were achieved and the films were verified as n-type by hard x-ray photoemission. Post-growth chlorine treatment (or $InCl_3$) was found to compensate the n-doping. Trial structures comprising CdS/CdTe:In verified that the doped absorber structures performed as expected both before and after chloride treatment, but it is recognized that this is not an optimum combination. Hence, in order to identify how the advantages of n-type absorbers might be fully realized in future work, we also report simulations of a range of p–n junction combinations with n-CdTe, a number of which have the potential for high V_{oc}.

1. Introduction

For the last 50 years in the development of p–n junction thin film photovoltaics, the device designs have been dominated by those with *p-type* absorbers, this being the case for both the commercially successful materials—CdTe and CIGS—and also for emerging materials such as CZTS. In this paper, we focus on an alternative device concept featuring n-type CdTe absorber layers. Devices with n-type absorbers have the potential for high performance arising from favorable material properties. Although we focus on CdTe, the concepts are likely to be translatable to other established and emerging materials systems.

The motivation for our interest in n-type absorbers is illustrated by the rationale for the conventional choice of p-type absorbers in thin film photovoltaics. The selection of p-type is essentially a default choice for the absorber since the window and transparent electrodes must comprise wide-gap semiconductors, and they can only be effectively doped n-type [1–3]. This demands that the absorber should be p-type to form a p–n junction with them. This combination is achievable in practice since semiconductors having the mid-range gaps required for solar absorbers can be doped p-type to complete the junction [1]. Therefore, the earliest CdTe solar cells were built in the nominal p–n configuration comprising glass/n-TCO/n-CdS/p-CdTe/contact. Industrially, the n-type transparent conducting oxide (TCO) is SnO_2:F (FTO) [4–6]. This device design reached a high point of ~16% PCE [7, 8] while the structures that evolved from it (i.e. omitting the CdS and including Cd(Se,Te) in the absorber) have reached 21% [9, 10]. All these devices

have p-type absorbers. The p-doping has most often been achieved by copper [11–19] but alternatives have been explored, including phosphorous [20] and more recently arsenic [21, 22], culminating in CdTe:As devices having PCEs > 20% [23].

Despite these successes, the use of p-type CdTe absorber layers present their own challenges related to doping and contacting. There is the potential to sidestep these by using n-type CdTe as follows: Firstly, doping—the efficiency of CdTe devices is limited by their open circuit voltage (V_{oc}), which is directly related to the achievable doping level [24]. While there is an upper limit for the stable n- or p-type doping density for any semiconductor [3], that limit is lower for p- than it is for n-CdTe. For example, the experimental data from Burst *et al* [25, 26] for CdTe:P shows a compensation crash at $p > 10^{17}$ cm^{-3}. (Marfaing [27] gives a detailed analysis of the phenomena.) On the other hand, stable n-type doping up to $n = 10^{18}$ cm^{-3} has been demonstrated using indium [28], this being close to the degenerate doping density and comfortably exceeding the levels required in PV devices. Secondly, contacting is a well-known issue for p-CdTe [29], and may create a back-contact barrier (from band line ups [30] or Fermi level pinning [31]) which limits the forward bias current of the devices [32]. Strategies, such as using ZnTe:Cu [33], are required to mitigate this barrier by supplying high local p-doping near the contact. Nevertheless, contacting to p-CdTe solar cells is found to be universally problematic, and a recent review identified more than 70 different strategies for making the contacts [29]. Whatever the origin of the difficulties for contacting p-CdTe, they are not an issue with n-type material, for which indium is known to give a low-resistance Ohmic contact [34, 35].

We therefore propose that re-designing the CdTe solar cell for an n-type absorber layer will provide options for manipulating the doping level and contacting that are not available from p-type. In particular, there may be opportunities for increasing V_{oc} and in simplifying contacting.

The key papers on the doping and properties of n-type and indium-doped CdTe include:

(a) Indium doping [28]: n-doping with In is achievable with close to 100% activation in single crystal CdTe up to ~10^{18} cm^3 after which V_{Cd} compensation sets in, followed by indium precipitation above 10^{20} cm^{-3}. The diffusion coefficient of indium is $D = 6.48 \times 10^{-4} \exp(-1.15\ \text{eV kT}^{-1})$ cm^2 s^{-1} at Te-saturation and $D = 117 \exp(-2.21\ \text{eV kT}^{-1})$ cm^2 s^{-1} at Cd-saturation. Segregation coefficients and the compensation mechanisms for indium in CdTe are comprehensively reviewed in Panchuk and Fochuk [36].

(b) Contacting [34]: low resistance contacts to single crystal n-CdTe may be formed with indium, providing the surface is oxide-free and the indium is thick enough, for example, 500 nm.

(c) Minority carrier lifetime and diffusion length: A range of values have been reported for τ_h in single crystal samples as follows: single crystal Bridgman—0.5 ns [37]; ion implanted single crystal—5.5 ns [38]; epitaxial MBE [39] and single crystal solvent evaporated 18.6 ns [39]. For polycrystalline CdTe grown under excess Te, the lifetime was measured as 7 ns [40]. The value of τ_h may well be a function of the doping density. Indeed, the minority carrier diffusion length L_h in single crystals drops in the range 2×10^{13}–8×10^{17} cm^{-3} according to the empirical relation:

$$\log(L_h) \approx 4.9 - 0.315 \log(n)^1. \quad (1)$$

Published reports of *thin film polycrystalline* devices having intentionally doped n-CdTe are limited to that from Palekis *et al* [41] who fabricated glass/TCO/CdS/CdTe:In/ZnTe devices having efficiencies up to 8.8%. The paper reports the effect on devices by varying the II/VI ratio in an elemental vapor delivery system, and of varying the amount of indium supplied to the substrate. No chloride processing was used.

There are also reports of n-CdTe in more complex junction devices: A series of papers from Arizona State University report MBE-growth of a unique ZnTe/CdTe/MgCdTe double heterostructure PV device demonstrating $V_{oc} > 1$ V, this being higher than for conventional CdTe devices [42–46]. Another work on MBE-grown epitaxial p-ZnTe/n-CdTe reports dark diode behavior, but no PV response [35]. Heterojunctions with n-CdTe have also been attempted on single crystal CdTe wafers coated with p-diamond (0.1%) [47], p–NiO_x (0.001%) [48] and MoO_x (no power conversion efficiency) [49, 50].

CdTe *homojunctions* have received little attention despite being ubiquitous in the traditional 'n-CdS/p-CdTe' device. It is well-known that the junction in these devices is a shallow homojunction in the CdTe, as demonstrated by electron beam induced current imaging [51]. Nevertheless, they are described as n-CdS/p-CdTe for convenience, and this is sometimes misunderstood [52]. The fabrication of doped homojunctions by MOCVD [22, 53] has been reported but with dark diode device results only. The modelling of intentionally doped shallow homojunction options has been reported by Song *et al* [54, 55].

In this work, we report post-growth doping trials using both indium metal and indium chloride with characterization by bulk and surface chemical analysis, near-surface band positions and carrier lifetime measurements. Photoemission measurements confirmed that indium imparted n-conductivity but that chlorine acted to compensate this. Accordingly, junctions based on CdS/CdTe had low efficiencies (~1%),

for indium-only doped CdTe, as would be expected for an n^+-n junction. Higher efficiencies were observed for chloride-treated material (∼10%), but given the observed compensation as a result of the chloride treatment, we do not consider this to be an n-CdTe based structure. As a result, we conclude the paper with modelling to evaluate future p–n device designs that have the potential to achieve high V_{oc}.

2. Experimental

2.1. Materials fabrication and doping

Thin films for the doping studies and for junction fabrication were prepared as follows: CdTe films were deposited by close space sublimation in a custom-built kit (Electro-gas Systems, Manchester). The source material was undoped 5 N CdTe (Alfa Aesar, particle size 0.5–4 mm), and the films were 3 μm thick. CdS was argon ion sputtered from a single source 5 N target (PiKem) in an AJA International Orion system. Au contacts were applied by evaporating 99.99% gold (Goodfellow). Substrates for device fabrication were NSG TEC15, a fluorine doped tin oxide (FTO) coated glass product having a sheet resistance of 15 $\Omega\,\square^{-1}$. Where chloride processing was applied to the finished devices, it was done by spraying aqueous $MgCl_2$ (99+% Alfa Aesar) followed by heating in air in a tube furnace at 410 °C after any doping had been done. Post-growth doping trials were conducted with two strategies, either (a) evaporation of indium metal directly onto the CdTe films (99.999% Sigma Aldrich) and annealing in a tube furnace under argon or (b) $InCl_3$ spray coating onto CdTe films in either an aqueous or methanolic solution (1 M solutions of 99.999% $InCl_3$ from Alfa Aesar) followed by annealing in air or under argon. Residues were removed using dilute nitric acid.

2.2. Materials characterization

X-ray diffraction was carried out using monochromated Cu-Kα_1 radiation in θ-2θ mode on a Rigaku Smart Lab system. X-ray photoelectron spectroscopy (XPS) of the surface chemistry of the films was undertaken at Harwell XPS. Calibration standards for the quantitative secondary ion mass spectroscopy (SIMS) measurement of indium in CdTe were prepared by implanting ^{115}In into single crystal CdTe wafers to a peak density of 10^{19} cm^{-3} at the Surrey Ion Beam Centre, UK. SIMS profiles were measured on a Cameca IMS 7f instrument by LSA Ltd.

Hot probe measurements were attempted on the films, with one contact being heated with a soldering iron to give a temperature gradient of 40 °C cm^{-1}. The currents were measured using a Keithley 2400 source meter on the 105 μA range and n-type InSb wafer was used as a reference. Hall measurements were attempted using a high sensitivity Semilab PDL Hall system at the University of Loughborough.

Hard x-ray photoemission spectroscopy (HAXPES) was performed on a beamline i09 at the Diamond Light Source synchrotron at Didcot, UK. Measurements were made using beam energies of 1.09, 2.2 and 6.6 keV in order to achieve a range of sampling depths. The core levels of Cd, Te, O and In were used to gain chemical information while the positions of the Fermi levels in the band gap were estimated by measuring the valence band (VB) edge relative to the Fermi level of a gold calibration specimen. Further details of the methods are reported by Hobson *et al* [56]. Both In-metal diffused and doped/$MgCl_2$-treated samples were measured, these being freshly prepared in the normal laboratory environment and transferred to the synchrotron in a vacuum suitcase system.

Carrier lifetime measurements were performed using an integrated Horiba time-correlated single photon counting system comprised of a DeltaDiode DD-650L 650 nm 100 MHz diode laser with a DeltaDiode controller and DeltaHub timing units. The excitation was performed through the glass to avoid any artefacts from free surface recombination. Time resolved photoluminescence (TRPL) signals were detected using a Horiba PPD-900 Si CCD-based picosecond photon detector mounted on a Horiba Jobin Yvon iHR320 fully automated spectrometer utilizing a 900 lines mm^{-1} diffraction grating. The decay signal for TRPL was selectively monitored at the peaks of near-gap CdTe emission. Data fitting was done using Horiba DAS-6 software. Standard PL spectra were measured using the 650 nm pulsed diode laser as an excitation source and collected using a Horiba Syncerity Si CCD detector.

2.3. Devices and device characterization

Trial structures based on a glass/FTO/n-CdS/n-CdTe/Au were fabricated using all of the different doping and chloride treatment protocols above. Current voltage (J–V) curves were measured using a Keithley 2400 source meter and when required, AAA AM1.5 illumination was provided at 1000 W m^{-2} by a TS Space Systems solar simulator. External quantum efficiency (EQE) measurements were made under white light bias using a Bentham PVE300 system. Capacitance–voltage (CV) measurements were used to determine carrier concentrations in the devices. Measurements were performed using a Solartron 1260 frequency response analyser with SmartLab software used to apply a 100 kHz frequency 30 mV AC perturbation voltage with the DC bias voltage sweep being from −1 to +1 V.

2.4. Simulations

Device simulations were performed with SCAPS Version 3.3.07, which is a one-dimensional solar cell simulation application developed at the Department of Electronics and Information Systems of the University of Gent, Belgium [57, 58]. This software is designed for thin film PV simulations and is based on the Poisson equation and the continuity equations for electrons and holes. A fulsome description of the simulation parameters used is given in the supplementary information.

3. Results

3.1. Chemical effects and indium incorporation in post-growth doped CdTe:In

Diffusion of In metal into CdTe surfaces did not leave any residue. However, use of either methanolic or aqueous $InCl_3$ left a white coating. Figures 1(a) and SI1 show the XPS survey spectra which have strong oxygen signals along with weaker signatures from indium and chlorine. The residue was sufficiently thick to allow XRD (figures 1(b) and SI2) and the principal peaks corresponded with those of InOCl (JCPDS 11-0510) [59]. This was considered to arise from the reaction [60]:

$$InCl_3 + H_2O \rightarrow InOCl + 2HCl$$

This reaction is known to occur above 280 °C, while further heat treatment at 400 °C > T > 900 °C for extended periods is known to yield In_2O_3 as follows: $3InOCl \rightarrow In_2O_3 + InCl_3$. Rinsing in 1 M HCl dissolved the InOCl and returned the XRD of the coated surfaces back to the standard pattern for CdTe (figure 1(b), bottom panel, JCPDS 15-0770). Hence the use of $InCl_3$ in *both* methanolic and aqueous solutions yielded InOCl—this being expected since methanol contains sufficient residual water to supply the reaction above.

Quantitative SIMS was used to check the incorporation of indium into the films. Figure 2 shows the profiles for films doped with indium metal only (200 °C and 400 °C for 20 min), a film that had been indium metal doped at 200 °C followed by $MgCl_2$ treatment (410 °C, 20 min) and an undoped control film with $MgCl_2$ treatment only. The 200 °C indium metal process gave a diffusion-like profile with a high signal near the free surface (left hand side, between 0 and 1 μm), before declining to the background signal level of 5×10^{15} cm^{-3} (the same background level as for the $MgCl_2$-only control). Indium metal doping at 200 °C followed by $MgCl_2$ treatment drove the indium to about 2.5 μm. Annealing without chlorine at the higher temperature of 400 °C gave flatter chemical densities of indium at the level of 10^{19} cm^{-3}. The peaks at the right-hand sides of the profiles are due to ^{115}Sn which is present in the underlying SnO_2 with a natural isotopic abundance of 0.34%. Comments on other features of the SIMS profiles are given in the supplementary information.

3.2. Carrier type and hard x-ray photoemission determination of Fermi level positions

Determination of the carrier type in polycrystalline CdTe films using transport methods is known to be difficult due to the adverse influence of the grain boundary fields. Nevertheless, we attempted both hot-probe and Hall measurements. While we were able to confirm n-type conductivity using the hot probe on large-grained (>5 mm) fragments of bulk CdTe:In, no reliable data could be obtained from any of the thin films prepared for this work. Similarly, high sensitivity Hall measurements made using both conventional and parallel dipole line systems failed to give a conclusive indication of the conductivity type.

Instead, we utilised HAXPES to determine the Fermi level positions which could then be used to infer the majority carrier type directly. Whereas conventional laboratory XPS is capable of Fermi level determination, we used a synchrotron hard x-ray source here to obtain depth-sensitive information: surface measurements may be compromised by surface band bending or else the surface chemistry. In this work, we used x-ray energies of 1.09, 2.2 and 6.6 keV at the Diamond Light Source i09 beamline in order to identify trends as a function of depth.

Figure 3 shows the variation in the apparent band positions for the two samples measured, i.e. those which had been (i) post-growth doped by diffusion of indium metal and (ii) doped and then treated with $MgCl_2$. The depth scale was obtained by estimating the escape depths of the photoelectrons as being twice the inelastic mean free paths (IMFP) using the IMFP data from Shinotsuka *et al* [61] and using the average of the photoelectron energies for Cd and Te $3d_{5/2}$, and $3d_{3/2}$ emissions for each energy (see figure SI3).

The trend line for the doped-only band positions in figure 3 shows an unexpected peak—such behaviour would be unphysical as a solution to Poisson's equation for a homogeneous semiconductor terminated by a charged surface. Hence, we considered the possible origins of this anomaly. First, we ruled out sample charging effects by monitoring the invariance of the C1s and core-level peaks. Secondly, we looked into systematic errors in the VB-edge fitting procedure. The data in the figure comes from applying a linear fit to the VB edge, with an example being shown in figure SI4. The uncertainty was <0.1 eV, which is less than the

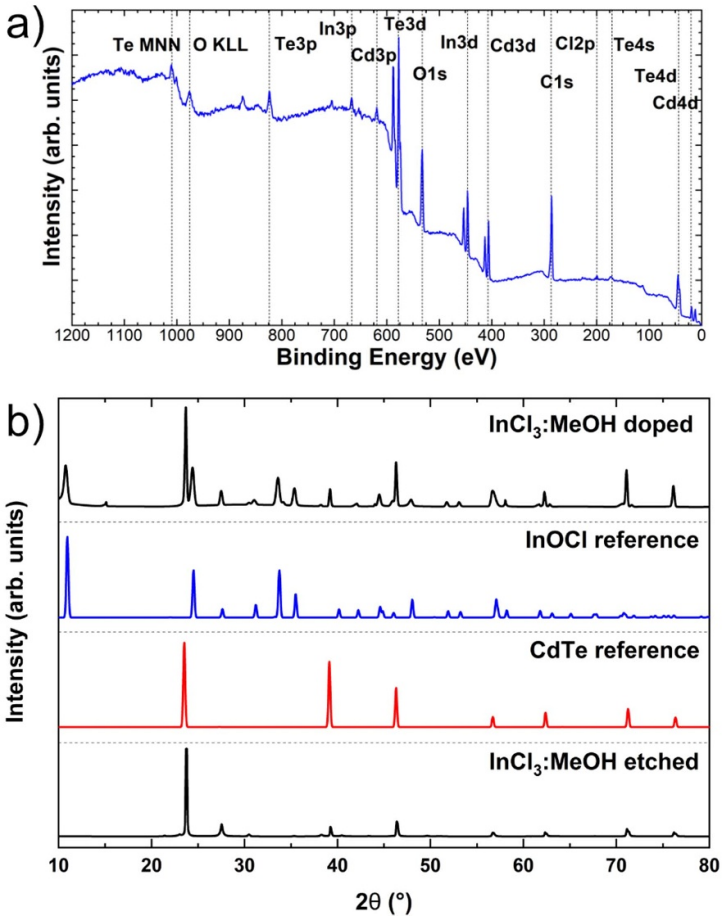

Figure 1. (a) XPS survey spectrum of a CdTe film that had been spray-coated with methanolic $InCl_3$ and heated in air at 400 °C for 20 min. There is strong oxygen contamination plus indium and a weak chlorine signal. (b) θ–2θ XRD pattern for a similar CdTe film (top). It corresponds with the peaks from InOCl and CdTe reference spectra (middle panels). This residue could be removed by etching with dilute acid to reveal the underlying CdTe (bottom).

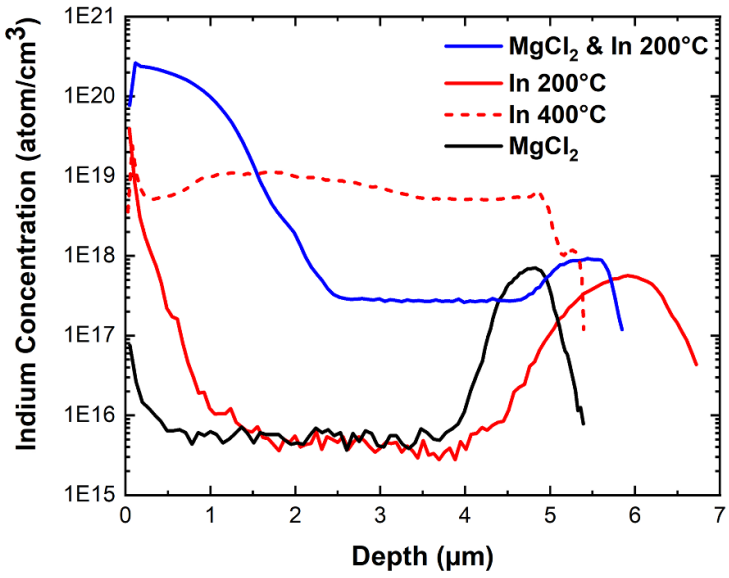

Figure 2. Quantitative SIMS profiles of ^{115}In in CdTe films post-growth doped with indium metal only and 200 °C and 400 °C, with indium metal at 200 °C followed by $MgCl_2$ and a $MgCl_2$-only control. The free surfaces of the CdTe are on the left while the peaks on the right are from ^{115}Sn (0.34% abundance).

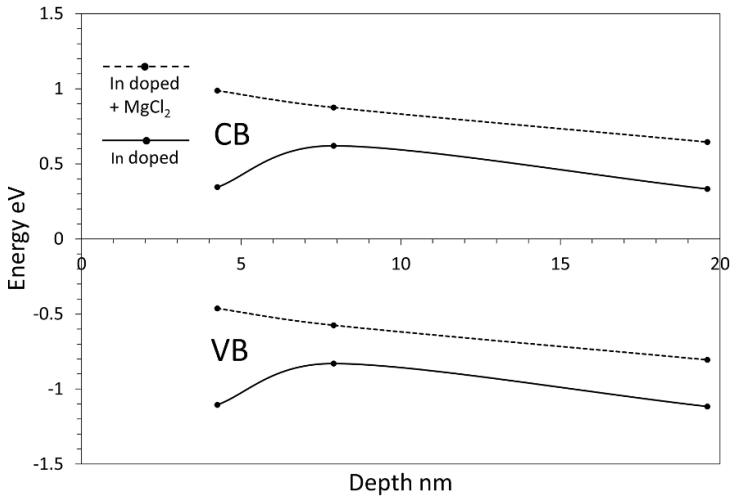

Figure 3. Band edge diagrams showing VB and CB positions using the Fermi level positions obtained from XPS and HAXPES at 1.09, 2.2 and 6.6 keV for CdTe samples that had been (i) post-growth doped by diffusion of indium metal and (ii) post-growth doped and then treated with $MgCl_2$. The Fermi level corresponds to 0 eV. The deepest two data points for each sample are the most reliable since they are not compromised of surface oxidation, as explained in the text.

difference between samples. Moreover, these results were comparable to those obtained from fitting the calculated VB DOS to the experimental spectra. Thirdly, and most tellingly, we estimated the near-surface oxide formation using the HAXPES core-level peaks and using photoelectron cross sections from Yeh and Lindau [62] (see figure SI5). For the doped sample, the ratio [O]/[Cd + Te] was 0.72 at the near-surface, falling to 0.29 and 0.23 for harder x-rays, while for the doped and chloride-treated sample it was 1.69, falling to 1.0 and 0.93 deeper in the sample. Recognising that these results represent convolutions over the escape depths (as opposed to true depth profiles), it remains clear in both cases that the near-surface measurements (1.09 keV) represent a more oxidised region than the deeper measurements (2.2 and 6.6 keV). We have therefore interpreted figure 3 using the data from these two deeper measurements only.

In both the doped and doped/chloride samples, the Fermi level measured with the highest energy x-rays is above mid-gap, indicating that they all have n-type characteristics. The In doped-only sample has the highest Fermi level position (0 eV in figure 3), this being consistent with n-doping. On the other hand, chloride treatment acts to depress the Fermi level, indicating that it acts to compensate the n-doping. In both cases, there is upward band bending towards the surface (disregarding the near surface data point for the oxidised region as explained above). Therefore, while all these photoemission measurements are surface-based, and so do not represent the true bulk materials behaviour, the trend is clear, and it is reasonable to conclude that the indium doping imparts n-type conductivity (indeed, this is borne out by the behaviour of the junction test structures reported in section 3.3).

3.3. Time resolved PL measurement of minority carrier lifetime

Figure 4 shows the room temperature PL spectra and decay curves obtained from CdTe films which were undoped (i.e. as grown) and post-growth doped with indium metal. All samples showed broad PL peaks which are consistent with the material being polycrystalline rather than single crystal. The strongest peaks were centered on ~820 nm (1.51 eV) which is close to the room temperature bandgap. This energy is consistent with the near-gap emission seen in, for example, high quality MBE-grown CdTe:In samples, although it is sharper at low temperatures [63].

The decay curves and their time constants are shown in figure 4 and table 1 respectively. For all samples, the time dependent PL decay was fitted to a two-component exponential:

$$I_{PL}(t) = A + B_1 e^{-\left(t/\tau_1\right)} + B_2 e^{-\left(t/\tau_2\right)}$$

where A is a background offset (fitting parameter), the process subscripted '1' is charge separation and that subscripted '2' represents minority carrier recombination. For these samples, the initial decay in the PL intensity in the first one or two nanoseconds is dominated by the fast component τ_1 (0.21–0.54 ns) while thereafter the curve shape matches that for the slower, bulk recombination, lifetime, τ_2, which falls in the range 1.5–2.5 ns. As expected, these values for polycrystalline material are all somewhat less than those reported for single crystal n-CdTe (5–20 ns) [37–40].

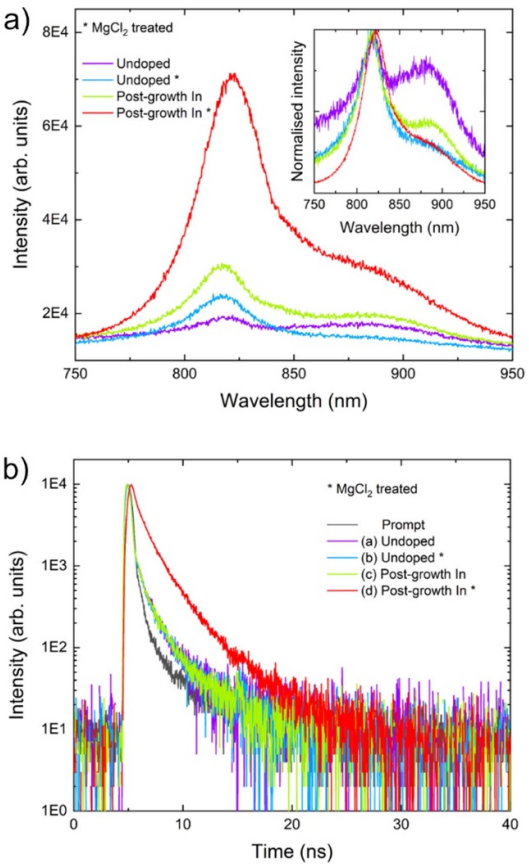

Figure 4. Photoluminescence data. (a) Room temperature PL spectra showing strong near band edge emission at ∼820 nm (∼1.51 eV) and weaker deeper luminescence at ∼890 nm (the inset shows the spectra normalized to the intense peak). (b) TRPL decay curves—the lifetimes are shown in table 1.

Table 1. TRPL lifetimes extracted from a double exponential fit to the data in figure 4.

Sample	τ_1 (ns)	τ_2 (ns)
(a) Undoped	0.22	1.49
(b) Undoped with $MgCl_2$	0.21	1.62
(c) Post-growth In	0.24	1.56
(d) Post-growth In with $MgCl_2$	0.54	2.51

3.4. CdS/CdTe:In junctions

To gain insight into how CdTe:In films performed in the context of a well-understood junction, we incorporated CdTe:In into 'traditional' CdS/CdTe junction designs. For example, it would be expected that n-type behavior in the CdTe would give a very weak junction when combined with CdS, which is n-type. We also examined the effects of chloride processing, for which the outcomes on CdTe:In in devices are unknown.

3.4.1. Junctions having CdTe post-growth doped with indium metal

Figure 5 shows the evolution of the CdS/CdTe:In solar cell performance parameters with the post-growth doping temperature in the range 200 °C–400 °C for 20 min diffusion time, plus an undoped control. (Shunt and series resistances are shown in figure SI6.)

Although there is a step up in V_{oc} from ∼0.2 to ∼0.4 V for the doped films compared to the undoped ones, all the performance parameters are low, and the average efficiency did not exceed 0.1%. The highest performing device achieved 0.24%, that being for doping at 400 °C. The reason for this low performance is explored in figure SI7 which shows the EQE responses for the same devices. All have a very low EQE response with a peak at the long wavelength (near-gap) end of the spectrum. This is characteristic of a buried junction which accounts for the very low photocurrents achieved.

Chloride treatment of indium-doped devices had the effect of increasing all performance parameters significantly: figures 6(a)–(d) show the working parameters of devices that had been first post-growth indium metal doped and then $MgCl_2$ treated at 410 °C for 20–60 min. There has been an increase of PCE

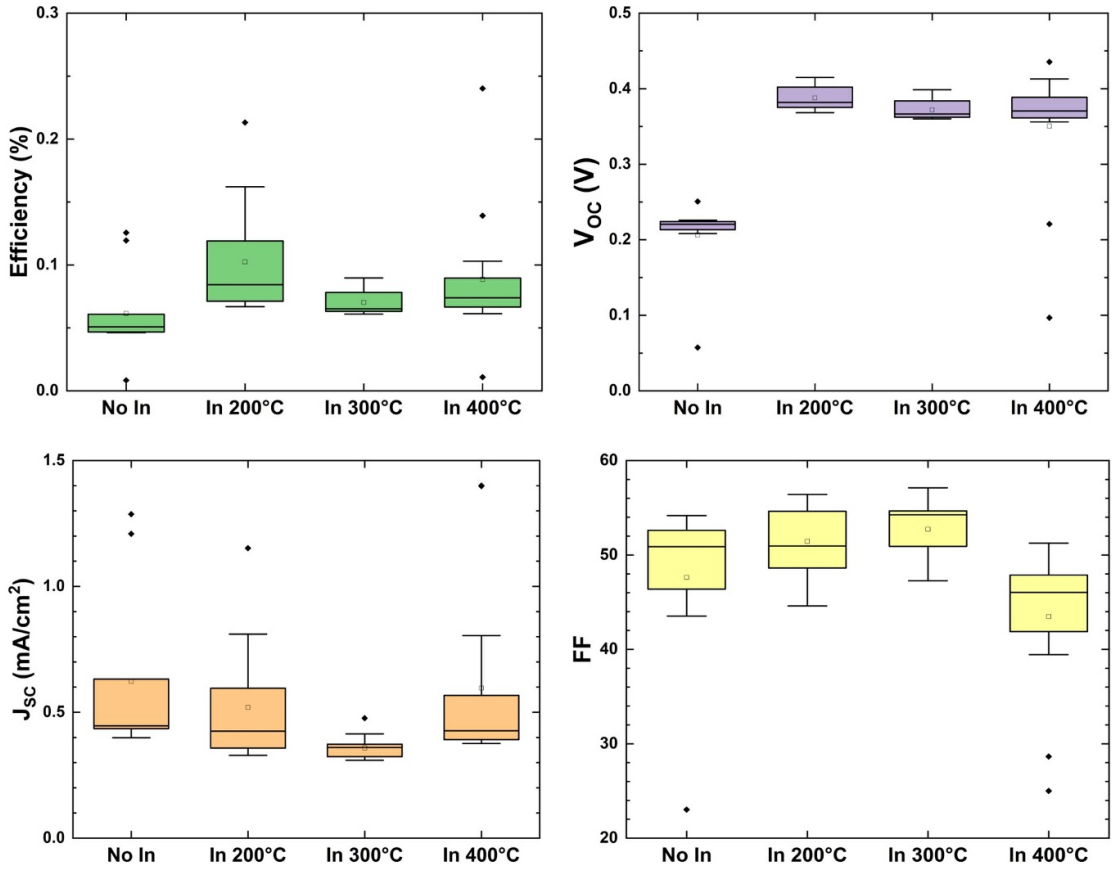

Figure 5. Performance parameters of glass/FTO/CdS/CdTe:In/Au devices in which the CdTe had been post-growth doped with indium metal at temperatures between 200 °C and 400 °C, plus a room temperature control. There was no chloride processing. $N = 16$ for each process.

from <0.5 to >10%. This increase is reflected in the change in the EQE shape from the buried junction seen for indium-only devices (figure SI7) to the shallow junction shape seen in figure 6(e). Moreover, the EQE shape for the chloride-treated devices very closely resembles that for a conventional CdS/CdTe device having copper doping and chloride processing, i.e. having a shoulder for wavelengths <500 nm due to parasitic absorption in the CdS and high collection between 600 nm and the bandgap cutoff. Repeat runs of the best processing conditions gave a peak performing cell having PCE = 10.3%, $V_{oc} = 0.74$ V, $J_{sc} = 25$ mA cm^{-2} and $FF = 55\%$, $R_{shunt} = 985\ \Omega$ and $R_{series} = 11.2\ \Omega$ as shown in figure 6(f). However, since the CdTe:In is known to be compensated by chlorine (section 3.1) this performance cannot be attributed to n-doping—a point which we discuss further in section 4.

3.4.2. Junctions having CdTe post-growth doped by diffusion of $InCl_3$

We conducted similar trials of CdS/CdTe junctions with $InCl_3$ processing in the temperature range 200 °C–400 °C. A temperature of 200 °C gave a buried junction EQE response as shown in figure SI8, with shallow junctions forming for higher temperatures. Hence temperatures in the range 390 °C–420 °C were explored in greater detail, with the device performance parameters being shown in figures 7(a)–(d) and their EQEs in figure SI9. The PV performance parameters did not change greatly in this temperature range but there was a peak in the C-V carrier concentration of $\sim 6 \times 10^{14}$ cm^{-3} for processing at 400 °C, which was twice that measured for the $MgCl_2$ control sample figure 7(e). (The C-V data is shown in figure SI10.) The highest performance for this series was a PCE of 9.6%, as shown in figure 7(f). Again, compensation of the n-doping by chlorine has generated a response similar to that of a traditional CdS/CdTe device and is discussed in section 4.

3.5. Modelling future concepts for n-CdTe devices

In order to realize the full potential of n-CdTe in devices we recognize that it will be necessary to deploy it in proper p–n junctions rather than the CdS/CdTe:In structures used in this work to gain initial insights. We therefore conclude this paper with a survey of potential device architectures and some SCAPS modelling of

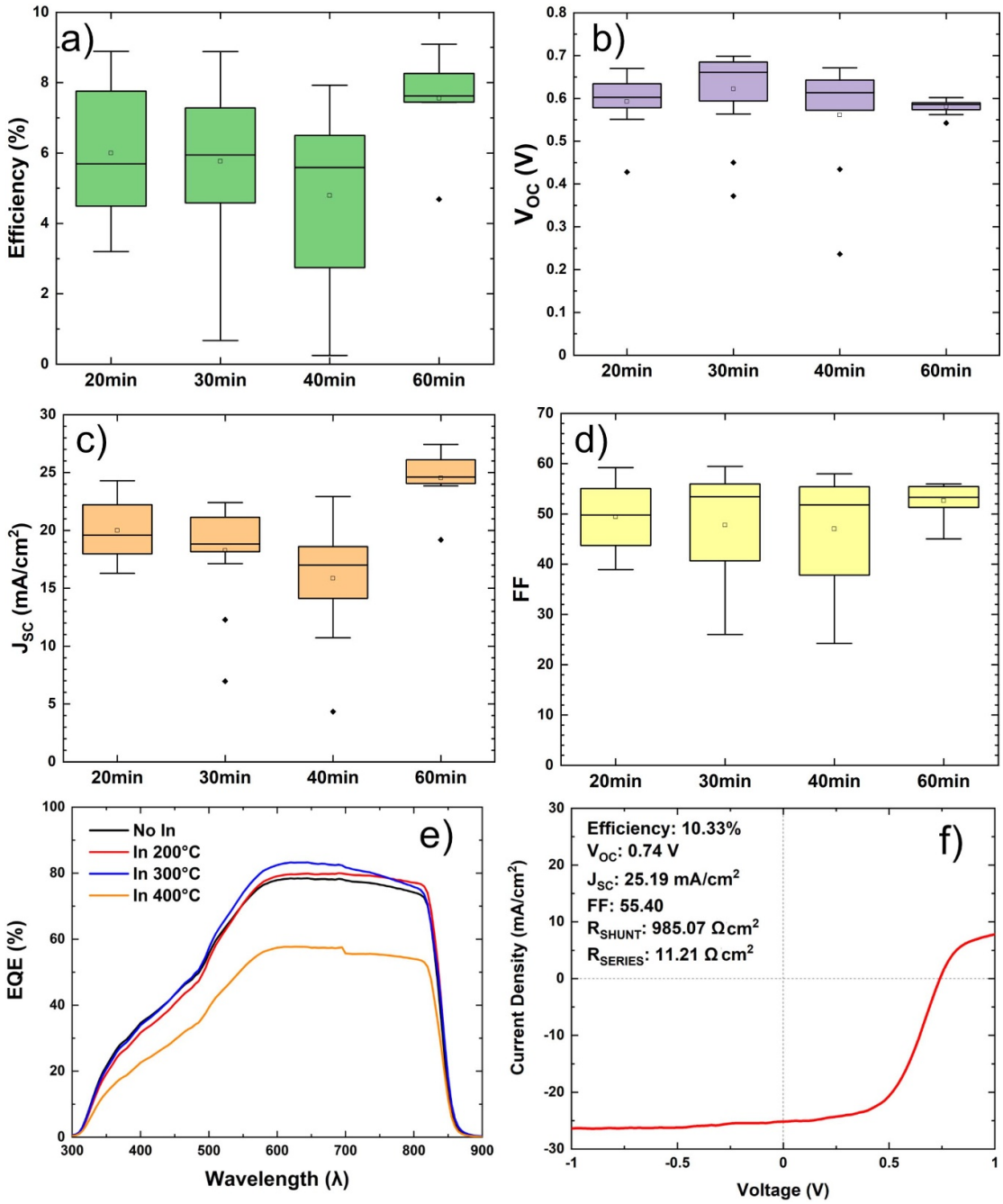

Figure 6. Data for glass/FTO/CdS/CdTe:In/Au devices that had been first doped by indium metal diffusion followed by $MgCl_2$ processing. (a)–(d) Performance parameters for chloride processing at 410 °C for the times shown ($N = 8$). (e) EQE responses for the devices which were chloride treated at 410 °C for 20 min as a function of the indium doping temperature. (f) AM1.5 *J–V* curve for the single highest efficiency device achieved by chloride processing at 410 °C in repeat runs.

specific designs. There are four basic alternatives, as shown in figure 8. They are (a) superstrate/n-uppermost, (b) superstrate/p-uppermost, (c) substrate/n-uppermost and (d) substrate/p-uppermost. Configurations (a) and (c), for which the n-type absorber is uppermost, have the advantage that light entering the junction does not have to first pass through a p-type semiconductor for which there will be optical losses.

We therefore trialled simulations of a wide range of device structures having the 'superstrate' configuration on FTO coated glass and with the light entering the n-CdTe before the p-type partner layer. Partner layers included i- and p-ZnTe, p-aSi, p-P3HT and p-CuI and also n-ZnO. We recognize that to make realistic models, it would be necessary to conduct extensive experiments to determine the bulk and interface trapping characteristics. Since that was out of the scope of this study, we instead included mid-gap traps in the model for all materials and having densities similar to those reported in the literature. Examples include: P3HT, 10^{13} cm^{-3}; ZnTe, 10^{13} cm^{-3}; CdTe, 10^{15} cm^{-3}; ZnO, 10^{15} cm^{-3} and FTO, 10^{15} cm^{-3} with full details of the material parameters being given in table SI1. The results of the modelling survey (table SI2) show a

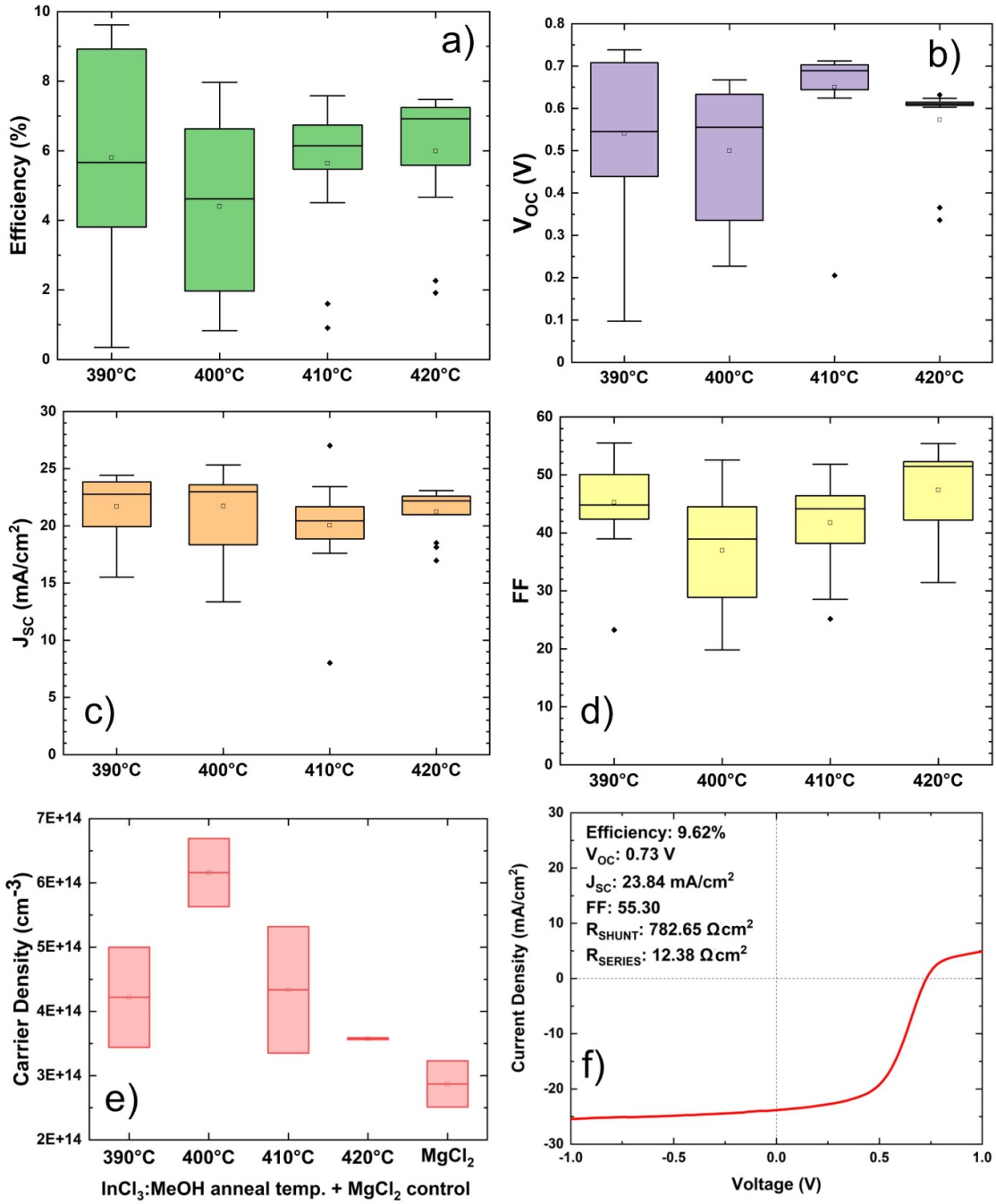

Figure 7. Data for glass/FTO/CdS/CdTe:In/Au devices prepared using a one-step post-growth doping/chloride treatment using $InCl_3$. (a)–(d) Performance parameters $N = 16$ (see figure SI9 for the EQE spectra). (e) Carrier densities for the devices processed using $InCl_3$ shown in (a)–(d), plus for an $MgCl_2$ control processed at 410 °C. (f) Light J–V curve for the highest performing single device fabricated using $InCl_3$.

selection of structures for which SCAPS modelling [57, 58] indicates $V_{oc} > 1$ V. For example, figure 9 shows the SCAPS-generated band diagram for glass/FTO/n-ZnO/n-CdTe/p-ZnTe/P3HT/Au and for which PCE = 24.6%; $V_{oc} = 1.1$ V; $J_{sc} = 30.2$ mA·cm^{-2} and $FF = 74.2\%$. This exercise gives some pointers to the structures for n-CdTe devices having the potential for high voltages and which may be worthy of future experimental investigation.

4. Discussion

We expected that n-doping of thin film polycrystalline CdTe would be feasible given the reports of it for single crystals [28, 64]. However, direct measurements using Hall and hot probe methods failed to confirm this and we speculate that this was due to grain boundary potentials. Nevertheless, HAXPES determinations of the Fermi level were able to identify n-type behavior for CdTe:In, with upward band bending near the

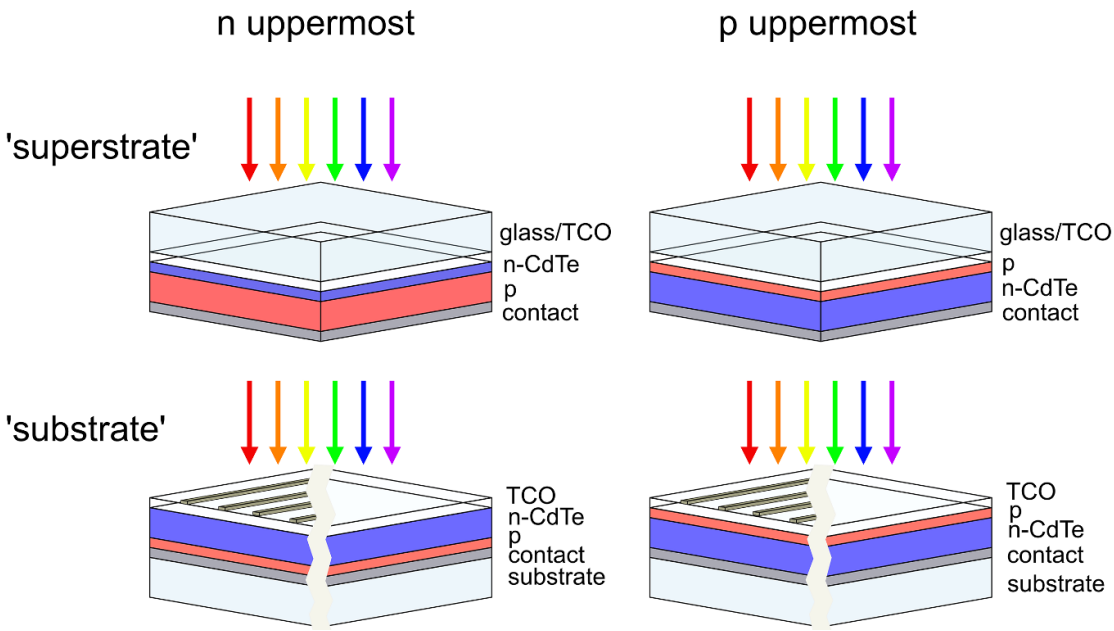

Figure 8. Device architectures using n-type absorbers. 'Superstrate' and 'substrate' geometries are possible in which the uppermost part of the p–n junction is either p- or n-type. For the 'substrate' versions, conductors may be required on the uppermost surfaces.

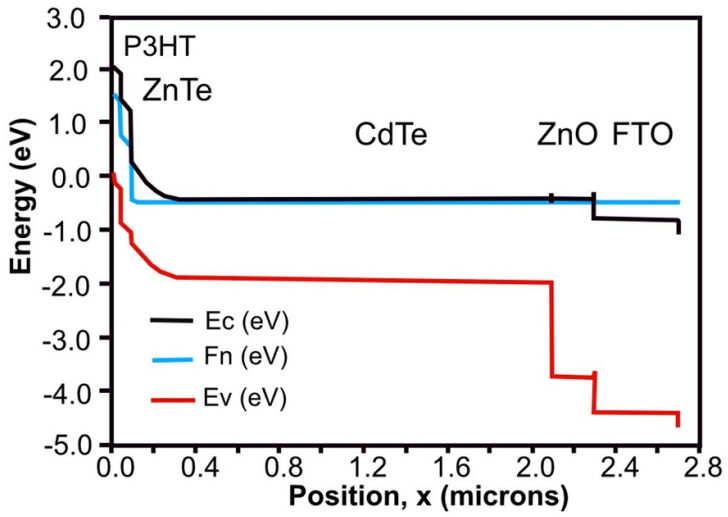

Figure 9. Simulated band diagram for a glass/FTO/n-ZnO/n-CdTe/p-ZnTe/P3HT/Au device. PCE = 24.9%; V_{oc} = 1.1 V; J_{sc} = 30.2 mA cm^{-2} and FF = 74.2%. Ec and Ev are the band edges while Fn is the Fermi level.

surface. However, C-V measurements of CdS/CdTe:In test structures indicated carrier concentrations of approximately 6×10^{14} cm^{-3}, while the chemical concentration was estimated as 10^{19} cm^{-3}. The low carrier activation is most likely due to compensation from over-doping, as described by Watson and Shaw [28]. Such compensation may also be responsible for the relatively low minority carrier lifetimes observed (~2.5 ns) although there are relatively few studies of lifetimes in n-type CdTe with which to compare.

Introduction of chlorides via $MgCl_2$ acted to depress the Fermi level indicating that chlorine acts to compensate the n-doping from indium. We know of no other specific study of co-doping or compensation in CdTe with both In and Cl. However, whereas other halogens are n-dopants, chlorine is known to have complex behaviour in CdTe and is used for compensating high resistivity CdTe for detectors [65]. In CdTe solar cells, it has been linked to 'type conversion' from n- to p-type [4, 5] to impart PV performance in junctions with n-CdTe [66]. (Grain boundary segregation of chlorine is also considered to impart grain boundary electrical passivation [67].) The CdS/CdTe:In test structures made here acted to confirm that the CdTe:In performed as might be expected from the above in the context of junctions. Indeed, the weak junction response for CdS/CdTe:In was consistent with there being an n–n junction. Compensation of the

CdTe:In with chlorine acted to strengthen the junction, but only to the level of a non-intentionally doped CdTe structure with chlorine treatment.

Hence, in order to realize the full potential of devices having n-CdTe absorbers, it will be necessary to make junctions having uncompensated n-CdTe with p-type partner layers. While SCAPS simulations (figures 8 and 9) have identified some possible candidate structures for which V_{oc} may exceed 1 V, we recognize the limitations of modelling in this respect. In particular, practical realization of devices having n-CdTe will have to overcome the issue of grain boundary passivation, namely that while chlorine effects passivation it would also compensate the n-doping. Further experimental investigations will be required to explore the device architecture and performance opportunities for n-CdTe.

Data availability statement

The data that support the findings of this study are openly available at the following URL/DOI: https://datacat.liverpool.ac.uk/id/eprint/1677.

Acknowledgments

The authors thank Keith Heaseman, Surrey Ion Beam Centre for ion implants and LSA Ltd for SIMS. Survey photoemission spectra were measured at the Harwell XPS EPSRC National Facility for XPS. HAXPES was conducted at the Diamond Light Source with the help of Tien-Lin Lee and Pardeep Kumar. Kerrie Morris, Mustafa Togay and Jake Bowers kindly ran the high sensitivity Hall measurements in Loughborough. Thanks also to Sean Kavanagh and David Scanlon of University College London for use of their calculated density of states data.

Funding

Funding from EPSRC contracts EP/T006188/1 and EP/L01551X/1 is gratefully acknowledged.

Conflict of interest

The authors know of no conflicts of interest related to this work.

Author contributions

L T undertook the majority of the film and device studies with additional contributions and advice from T D C H and L J P. K J C and N T performed the simulations. S C and V B were responsible for the TRPL. M I carried out the chemical XPS while H S conducted the XPS determination of band positions under the supervision of T D V and V D. L T, T D C H, L J P, L A H J, M J S, C H D, K D and T D V all contributed to taking the HAXPES measurements. J D M advised on the research methodology and interpretations. K D designed the study and wrote the manuscript while all authors commented or advised.

ORCID iDs

Theo D C Hobson https://orcid.org/0000-0002-0013-360X
Kieran J Cheetham https://orcid.org/0000-0002-3534-2049
Matt J Smiles https://orcid.org/0000-0003-2530-5647
Tim Veal https://orcid.org/0000-0002-0610-5626
Ken Durose https://orcid.org/0000-0003-1183-3211

References

[1] Becker C R 2009 *CdTe and Related Compounds: Physics, Defects, Technology, Hetero- and Nanostructures and Applications Part I. Physics, CdTe-based Nanostructures, CdTe-based Semimagnetic Semiconductors, Defects* ed R Triboulet and P Siffert (Amsterdam: Elsevier)
[2] Faschinger W 1999 Doping and contacting of wide gap II–VI compounds *J. Cryst. Growth* **197** 557
[3] Walukiewicz W 2001 Intrinsic limitations to the doping of wide-gap semiconductors *Physica* B **302** 123
[4] Basol B M 1984 High-efficiency electroplated heterojunction solar-cell *J. Appl. Phys.* **55** 601
[5] Basol B M, Ou S S and Stafsudd O M 1985 Type conversion, contacts, and surface effects in electroplated CdTe films *J. Appl. Phys.* **58** 3803
[6] Bonnet D and Rabenhorst H 1972 *Proc. 9th IEEE Photovoltaic Specialists Conf.* (*Silver Springs, MD*) p 129
[7] Britt J and Ferekides C 1993 Thin-film CdS/CdTe solar-cell with 15.8% efficiency *Appl. Phys. Lett.* **62** 2851

[8] Wu X Z 2004 High-efficiency polycrystalline CdTe thin-film solar cells *Sol. Energy* **77** 803
[9] Green M, Dunlop E, Hohl-Ebinger J, Yoshita M, Kopidakis N and Hao X J 2021 Solar cell efficiency tables (version 57) *Prog. Photovolt.* **29** 3
[10] First solar press release 2014 (available at: https://investor.firstsolar.com/news/press-release-details/2014/First-Solar-Builds-the-Highest-Efficiency-Thin-Film-PV-Cell-on-Record/default.aspx) (Accessed April 2022)
[11] Emziane M, Durose K, Bosio A, Romeo N and Halliday D P 2005 Effect of the purity of CdTe starting material on the impurity profile in CdTe/CdS solar cell structures *J. Mater. Sci.* **40** 1327
[12] Emziane M, Durose K, Halliday D P, Bosio A and Romeo N 2005 Role of substrate and transparent conducting oxide in impurity evolvement in polycrystalline thin-film devices *Appl. Phys. Lett.* **87** 1
[13] Emziane M, Durose K, Halliday D P, Bosio A and Romeo N 2005 Efficiency improvement in thin-film solar cell devices with oxygen-containing absorber layer *Appl. Phys. Lett.* **87** 1
[14] Emziane M, Durose K, Halliday D P, Bosio A and Romeo N 2005 *Materials Research Society Symp. Proc. Materials Research Society Spring Meeting* (*San Francisco, CA, 29 March 2005–1 April 2005*) vol 865 p F14.11
[15] Emziane M, Durose K, Halliday D P, Romeo N and Bosio A 2005 The distribution of impurities in the interfaces and window layers of thin-film solar cells *J. Appl. Phys.* **97** 114910
[16] Emziane M, Durose K, Romeo N, Bosio A and Halliday D P 2005 Effect of $CdCl_2$ activation on the impurity distribution in CdTe/CdS solar cell structures *Thin Solid Films* **480–481** 377
[17] Emziane M, Durose K, Romeo N, Bosio A and Halliday D P 2005 A combined SIMS and ICPMS investigation of the origin and distribution of potentially electrically active impurities in CdTe/CdS solar cell structures *Semicond. Sci. Technol.* **20** 434
[18] Emziane M, Halliday D P, Durose K, Romeo N and Bosio A 2007 On the origins of impurities in CdTe-based thin film solar cells *MRS Online Proc. Library* **1012** 334
[19] Emziane M, Ottley C J, Durose K and Halliday D P 2004 Impurity analysis of $CdCl_2$ used for thermal activation of CdTe-based solar cells *J. Phys. D: Appl. Phys.* **37** 2962
[20] Alnajjar A A, Watson C C R, Brinkman A W and Durose K 1992 Post-growth doping of bulk CdTe crystals with phosphorus *J. Cryst. Growth* **117** 385
[21] Berrigan R A, Maung N, Irvine S J C, Cole-Hamilton D J and Ellis D 1998 Thin films of CdTe/CdS grown by MOCVD for photovoltaics *J. Cryst. Growth* **195** 718
[22] Taskar N R, Natarajan V, Bhat I B and Ghandi S K 1988 Extrinsic doped n- and p-type CdTe layers grown by organometallic vapour phase epitaxy *J. Cryst. Growth* **86** 228–32
[23] Metzger W K *et al* 2019 Exceeding 20% efficiency with *in situ* group V doping in polycrystalline CdTe solar cells *Nat. Energy* **4** 837
[24] Sites J and Pan J 2007 Strategies to increase CdTe solar-cell voltage *Thin Solid Films* **515** 6099
[25] Burst J M *et al* 2016 CdTe solar cells with open-circuit voltage breaking the 1V barrier *Nat. Energy* **1** 16015
[26] Burst J M, Farrell S B, Albin D S, Colegrove E, Reese M O, Duenow J N, Kuciauskas D and Metzger W K 2016 Carrier density and lifetime for different dopants in single-crystal and polycrystalline CdTe *APL Mater.* **4** 6
[27] Marfaing Y 1981 Self-compensation in II–VI compounds *Prog. Cryst. Growth Charact. Mater.* **4** 317
[28] Watson E and Shaw D 1983 The solubility and diffusivity of In in CdTe *J. Phys.* C **16** 515
[29] Hall R S, Lamb D and Irvine S J C 2021 Back contacts materials used in thin film CdTe solar cells-A review *Energy Sci. Eng.* **9** 606
[30] Brinkman A W 2010 *CdTe and Related Compounds; Physics, Defects, Hetero- and Nano-Structures, Crystal Growth, Surfaces and Applications, Part II: Crystal Growth, Surfaces and Applications* ed R Triboulet and P Siffert (Amsterdam: Elsevier Science Bv)
[31] Pan J, Gloeckler M and Sites J 2006 Hole current impedance and electron current enhancement by back-contact barriers in CdTe thin-film solar cells *J. Appl. Phys.* **100** 124505
[32] Stollwerck G and Sites J R 1995 *13th European Photovoltaic Solar Energy Conf.* (Nice: WIP)
[33] Gessert T A, Mason A R, Sheldon P, Swartzlander A B, Niles D and Coutts T J 1996 Development of Cu-doped ZnTe as a back-contact interface layer for thin-film CdS/CdTe solar cells *J. Vac. Sci. Technol.* A **14** 806
[34] Braithwaite R E and Mullin J B 1980 Formation and stability of In contacts to n-type CdTe *Solid-State Electron.* **23** 1091
[35] Chusnutdinow S, Makhniy V P, Wojtowicz T and Karczewski G 2012 Electrical properties of p-ZnTe/n-CdTe photodiodes *Acta Phys. Pol.* A **122** 1077
[36] Panchuk O and Fochuk P 2009 *CdTe and Related Compounds; Physics, Defects, Hetero- and Nano-structures, Crystal Growth, Surfaces and Applications* vol Part I (Amsterdam: Elsevier)
[37] Cusano D A and Lorenz M R 1964 CdTe hole lifetime from the photovoltaic effect *Solid State Commun.* **2** 125
[38] Chu M, Fahrenbruch A L, Bube R H and Gibbons J F 1978 Photo-voltaic properties of CdTe p–n junctions produced by ion-implantation *J. Appl. Phys.* **49** 322
[39] Wight D R, Bradley D, Williams G, Astles M, Irvine S J C and Jones C A 1982 Minority-carrier diffusion length in CdTe *J. Cryst. Growth* **59** 323
[40] Khan I S, Evani V K, Palekis V and Ferekides C 2017 Effect of stoichiometry on the lifetime and doping concentration of polycrystalline CdTe *IEEE J. Photovolt.* **7** 1450
[41] Palekis V, Khan I, Collins S, Hsu C A, Misra S, Scarpulla M A, Zhang Y H, Morel D and Ferekides C 2018 *2018 IEEE 7th World Conf. on Photovoltaic Energy Conversion* (New York: IEEE)
[42] Kuo Y S, Becker J, Liu S, Zhao Y, Zhao X H, Su P Y, Bhat I and Zhang Y H 2015 *2015 IEEE 42nd Photovoltaic Specialist Conf.* (New York: IEEE)
[43] Zhao X H, DiNezza M J, Liu S, Campbell C M, Zhao Y and Zhang Y H 2014 Determination of CdTe bulk carrier lifetime and interface recombination velocity of CdTe/MgCdTe double heterostructures grown by molecular beam epitaxy *Appl. Phys. Lett.* **105** 4
[44] Zhao X-H, DiNezza M J, Liu S, Lin S, Zhao Y and Zhang Y-H 2014 Time-resolved and excitation-dependent photoluminescence study of CdTe/MgCdTe double heterostructures grown by molecular beam epitaxy *J. Vac. Sci. Technol.* B **32** 040601
[45] Zhao X H, Liu S, Zhao Y, Campbell C M, Lassise M B, Kuo Y S and Zhang Y H 2016 Electrical and optical properties of n-type indium-doped CdTe/$Mg_{0.46}Cd_{0.54}Te$ double heterostructures *IEEE J. Photovolt.* **6** 552
[46] Zhao Y, Boccard M, Liu S, Becker J, Zhao X H, Campbell C M, Suarez E, Lassise M B, Holman Z and Zhang Y H 2016 Monocrystalline CdTe solar cells with open-circuit voltage over 1V and efficiency of 17% *Nat. Energy* **1** 7
[47] von Huth P, Butler J E and Tenne R 2001 Diamond/CdTe: a new inverted heterojunction CdTe thin film solar cell *Sol. Energy Mater. Sol. Cells* **69** 381
[48] Parkhomenko H, Solovan M, Brus V, Maystruk E and Maryanchuk P 2018 Structural, electrical, and photoelectric properties of p-NiO/n-CdTe heterojunctions *Opt. Eng., Bellingham* **57** 5

[49] Solovan M M, Brus V V, Mostovyi A I, Maryanchuk P D, Tresso E and Gavaleshko N M 2016 Molybdenum oxide thin films in CdTe-based electronic and optoelectronic devices *Phys. Status Solidi* **10** 346
[50] Solovan M M, Gavaleshko N M, Brus V V, Mostovyi A I, Maryanchuk P D and Tresso E 2016 Fabrication and investigation of photosensitive MoO_x/n-CdTe heterojunctions *Semicond. Sci. Technol.* **31** 6
[51] Major J D, Bowen L, Treharne R and Durose K 2014 Assessment of photovoltaic junction position using combined focused ion beam and electron beam-induced current analysis of close space sublimation deposited CdTe solar cells *Prog. Photovolt.* **22** 1096
[52] Dharmadasa I M, Alam A E, Ojo A A and Echendu O K 2019 Scientific complications and controversies noted in the field of CdS/CdTe thin film solar cells and the way forward for further development *J. Mater. Sci., Mater. Electron.* **30** 20330
[53] Su P Y, Dahal R, Wang G C, Zhang S B, Lu T M and Bhat I B 2015 Single-crystal CdTe homojunction structures for solar cell applications *J. Electron. Mater.* **44** 3118
[54] Song T, Kanevce A and Sites J R 2016 Emitter/absorber interface of CdTe solar cells *J. Appl. Phys.* **119** 8
[55] Song T, Kanevce A and Sites J R 2016 *2016 IEEE 43rd Photovoltaic Specialists Conf.* (New York: IEEE)
[56] Hobson T D C *et al* 2020 Isotype heterojunction solar cells using n-type Sb_2Se_3 thin films *Chem. Mat.* **32** 2621
[57] Burgelman M, Nollet P and Degrave S 2000 Modelling polycrystalline semiconductor solar cells *Thin Solid Films* **361** 527
[58] Burgelman M, Verschraegen J, Degrave S and Nollet P 2004 Modeling thin-film PV devices *Prog. Photovolt.* **12** 143
[59] Forsberg H E 1956 The crystal structure of indium oxide chloride and indium oxide bromide *Acta Chem. Scand.* **10** 1287
[60] Yang H Q, Zhao H, Dong H X, Yang W Y and Chen D C 2009 Preparation of In_2O_3 octahedrons by heating $InCl_3$ aqueous solution on the Si substrate *Mater. Res. Bull.* **44** 1148
[61] Shinotsuka H, Tanuma S, Powell C J and Penn D R 2018 Calculations of electron inelastic mean free paths. XII. Data for 42 inorganic compounds over the 50 eV to 200 keV range with the full Penn algorithm *Surf. Interface Anal.* **51** 427
[62] Yeh J J and Lindau I 1985 Atomic subshell photoionization cross sections and asymmetry parameters: $1 \leqslant Z \leqslant 103$ *At. Data Nucl. Data Tables* **32** 1
[63] Bicknell R N, Giles N C and Schetzina J F 1986 Growth of high mobility n-type CdTe by photoassisted molecular-beam epitaxy *Appl. Phys. Lett.* **49** 1095
[64] Segall B, Halsted R E and Lorenz M R 1963 Electrical properties of n-type CdTe *Phys. Rev.* **129** 2471
[65] Agrinskaya N V and Matveev O A 1975 Electrical-properties of In-doped and Cl-doped CdTe cyrstals with a correlated impurity distribution *Sov. Phys. Semicond. USSR* **9** 1423
[66] AlAllak H M, Brinkman A W, Richter H and Bonnet D 1996 Dependence of CdS/CdTe thin film solar cell characteristics on the processing conditions *J. Cryst. Growth* **159** 910
[67] Major J D, Al Turkestani M, Bowen L, Brossard M, Li C, Lagoudakis P, Pennycook S J, Phillips L J, Treharne R E and Durose K 2016 In-depth analysis of chloride treatments for thin-film CdTe solar cells *Nat. Commun.* **7** 10